A micromechanism study of thermosonic gold wire bonding on aluminum pad

H. Xu,[1,2,a)] C. Liu,[1] V. V. Silberschmidt,[1] S. S. Pramana,[3] T. J. White,[3,4] Z. Chen,[3] M. Sivakumar,[5] and V. L. Acoff[2]
[1]*Wolfson School of Mechanical and Manufacturing Engineering, Loughborough University, Loughborough, LE11 3TU, United Kingdom*
[2]*Department of Metallurgical and Materials Engineering, The University of Alabama, Tuscaloosa, Alabama 35487, USA*
[3]*School of Materials Science and Engineering, Nanyang Technological University, Nanyang Avenue, Singapore 639798*
[4]*Centre for Advanced Microscopy, Australian National University, Canberra ACT 2601, Australia*
[5]*ASM Technology Singapore, 2 Yishun Avenue 7, Singapore 768924*

(Received 5 July 2010; accepted 8 October 2010; published online 8 December 2010)

A micromechanism of thermosonic gold wire bonding was elaborated by examining its interfacial characteristics as a result of the bonding process, including the fragmentation of the native aluminum oxide layer on Al pads, and formation of initial intermetallic compounds (IMCs). It is found that the existence of an approximately 5 nm thick native oxide layer on original Al pads has a significant effect on the bonding, and the nucleation of IMCs during the bonding process must overcome this relatively inert thin film. Bonding strength was fundamentally determined by the degree of fragmentation of the oxide films, through which the formation of IMCs can be initiated due to the direct contact of the metal surfaces to be bonded. The extent of fracture the oxide layer was strongly influenced by the level of ultrasonic power, as at its high level alumina fragmentation becomes pervasive resulting in contiguous alloy interfaces and robust bonds. The IMCs formed at the interfaces were identified as Al_4Al and $AuAl_2$ with a thickness of 150–300 nm. The formation mechanism of such IMCs was explained by the effective heat of formation theory.
 [doi:10.1063/1.3514005]

I. INTRODUCTION

Thermosonic gold wire bonding is broadly used for electronic interconnects. In this process, a thin gold wire is attached to an aluminum metallization pad using a combination of ultrasonic energy, pressure (~140 MPa) and heat (150–220 °C), to initiate a complex solid state reaction of fundamental technological importance. The mechanisms traditionally used to describe bonding are fretting[1] and microslip.[2,3] During fretting interfacial sliding cleans and heats the wire and pad surfaces, while in the microslip model localized rather than gross interfacial motion is emphasized; both descriptions assume that removal of a ubiquitous native alumina overlayer is essential for successful bonding as it will act as a barrier to diffusion, but to date, this has not been verified experimentally.

Ultrasonics enhance bonding. Langenecker[4] found aluminum single crystal elongation when exposed to 20 kHz vibration at constant temperature (18 °C) proved equivalent to the morphological changes accompanying heating alone. However, the ultrasonic energy density required for deformation was $\sim 10^7$ times less than by thermal energy (for example, an ultrasonic energy of 35 W cm^{-2} is equivalent to 600 °C). Harman[5] reported that ultrasonic treatment activated dislocation formation and migration in metal pads and wires, with the beneficial influence on bonding strength being well documented.[6–8] Nonetheless, a full account of the underlying mechanistic aspects has not been presented.

Intermetallic compound (IMC) crystallization at the Au–Al interface is essential to form a strong bond. According to an early Au–Al equilibrium phase diagram,[9] five IMCs—$AuAl_2$, AuAl, Au_2Al, Au_5Al_2, and Au_4Al—possibly exist. However, subsequent studies have revealed greater complexity, including polymorphism and metastable phases[10–25] (Table I). Au_4Al is at least trimorphic and exists in the cubic β ($Im\bar{3}m$) (Ref. 16) and β' ($P2_13$) (Refs. 13–15) forms; a third tetragonal polymorph ($I4/mmm$) (Ref. 17) has been reported. The phase initially identified as Au_5Al_2 was, subsequently, shown by Range and Buechler[18] to be Au_8Al_3, a complex rhombohedral structure $R\bar{3}c$ of large unit cell. Definitive crystallographic data for Au_5Al_2 has not been collected, and its existence is speculative, despite frequent reference to this compound. Consequently, previous x-ray diffraction studies of the Au–Al system using thin film couples[28–30] suggesting that "Au_5Al_2" nucleates first, followed by Au_2Al or Au_4Al, should be considered in this light; the substantial difficulties of Francombe *et al.*[31] in isolating the rhombohedral phase by electron diffraction are noted. Interfacial reactions during wire bonding are inherently nonequilibrium processes, with the possibility of quenching metastable compounds. In general, high symmetry alloys with small unit cells will easily crystallize, while long range ordered and low symmetry phases are less likely to form during bonding. Therefore, Au_8Al_3 (often mislabelled as

a)Electronic mail: hxu14@bama.ua.edu and huixu.hit@gmail.com.

TABLE I. Crystallographic data for compounds and polymorphs of the Au–Al system. The data quality is variable, with single crystal x-ray diffraction being more reliable than powder methods. Electron diffraction is least compelling, not supplemented by quantitative chemical microanalysis, and usually collected from metal couplings that are quenched and far from equilibrium. The thermodynamic data ($\Delta H°$) (Ref. 26) is assumed consistent with the highest symmetry and smallest unit cell polymorph stable under ambient conditions. The effective heat of formation ΔH were calculated at the composition with the lowest eutectic temperature (78 at. % Au and 22 at. % Al) (Ref. 27). $\Delta H'$ were calculated at the effective composition of 67 at. % Au and 33 at. % Al near the aluminum pad, while $\Delta H''$ at 80 at. % Au and 20 at. % Al was assumed adjacent the gold wire.

Chemistry		Crystallochemical parameters				Thermodynamic parameters				
Composition[a]	Au:Al	Polymorph/ compound symmetry	Space group	Atoms per unit cell	Unit cell volume (Å^3)	$\Delta H°$ [b] (kJ/mol)	ΔH (Pretorius *et al.*) (kJ/mol)	$\Delta H'$ (near Al pad) (kJ/mol)	$\Delta H''$ (near Au wire) (kJ/mol)	Structure reference
$Au_{23}Al$	23	Cubic	$Fm\bar{3}m$	4	67.28[c]					10
$Au_{86}Al_{14}$	6.14	Cubic	$Fm\bar{3}m$	4	66.85[c]					11 and 12
Au_4Al	4	Cubic (β')	$P2_13$	20	331.76[c,d]	−19	−18.5	−7.8	−19.0	13–15
		Cubic (β)	$Im\bar{3}m$	2	34.01[e,f]					16
		Tetragonal	$I4/mmm$	2	33.02[c,g]					17
Au_8Al_3 [h]	2.66	Rhombohedral	$R\bar{3}c$	44	724.77[i,f]	−26	−20.0	−11.9	−18.2	18
Au_2Al	2	Orthorhombic	$Pnma$	12	190.54[c,j]	−30	−19.8	−14.8	−18.0	19
		Orthorhombic	$Pnnm$	30	475.16[c,k]					19
AuAl	1	Cubic	$Pm\bar{3}m$	2	30.96[e]	−37	−16.3	−24.4	−14.8	20
$AuAl_2$		Monoclinic	$P2_1/m$	32	135.26[i]					21 and 22
	0.5	Cubic	$Fm\bar{3}m$	12	215.71[c]	−31	−10.2	−30.7	−9.3	22–25

[a]These compositions are idealized, but as wire bonding is a quenching reaction a range of compounds, with the same high symmetry will likely be crystallized. Longer range order, and lower symmetries are less likely to form during bonding.
[b]ΔH values are with respect to the smallest unit cell showing the shortest range order.
[c]Powder x-ray diffraction.
[d]Stable from 690–810 K.
[e]Electron diffraction.
[f]Synthesized at 2 GPa, 1473 K.
[g]Metastable.
[h]Au_8Al_3 is the correct composition and structure determined by Range and Buechler[18] but first identified by Francombe *et al.*[31] using electron diffraction as Au_5Al_2 (Au:Al=2.5). While there are frequent literature references to Au_5Al_2 there is, as yet, no definitive proof of its existence. Pretorius *et al.*[27] assumed Au_5Al_2 for determining ΔH.
[i]Single crystal x-ray diffraction.
[j]Stable below 838 K.
[k]Stable below 848 K.

Au_5Al_2) has the most extensive order of any Au–Al alloy confirmed to date (44 atoms per unit cell) and anticipated to rarely appear during thermosonic bonding. Small unit cell volume IMCs such as ordered (Au_4Al, $P2_13$, 20 atoms per unit cell) and disordered ($Au_{23}Al$, $Fm\bar{3}m$, 4 atoms per unit cell) are expected to be prevalent.

In this paper, the evolution of amorphous aluminum oxide encapsulating the aluminum pad is monitored by high resolution transmission electron microscopy (HRTEM) to directly clarify its role during bonding. It is found that fracture of this outer alumina film promotes the formation of IMCs, whose integrity correlates with ultrasonic energy, interfacial structure and bonding strength. IMCs in gold wire bonds are crystallochemically described as Au_4Al and $AuAl_2$, and the manner by which amorphous alumina controls Au and Al interfacial concentrations and interdiffusion are examined explicitly.

II. EXPERIMENTAL METHODS

Thermosonic gold wire bonding employed an ASM Eagle 60AP ball/wedge automatic bonder. The gold wire (99.99 wt %) was 20 μm in diameter with an elongation of 2%–6%. A silicon chip patterned with 1 μm thick sputtered aluminum pads was loaded on a work stage. An electrical flame off process with a 40 mA current, 4500 V gap voltage and 230 μs discharge time produced a free air ball at the gold wire tip. After cooling, the gold ball was transferred onto a pad to form the Au–Al bond using a combination of a normal force, transverse ultrasonic vibration and heat (Table II). Three ultrasonic power settings (levels 1, 2, and 3) at a fixed frequency of 138 kHz were used to investigate the effect of vibration on the Au–Al interfacial structure and bonding strength. Because ultrasonic power developed in the piezoceramic stack was transferred with loss, the actual ultrasonic amplitudes at the capillary tip were measured by laser interferometery (Table II). To reduce post-thermal ef-

TABLE II. Thermosonic bonding parameters.

Bonding parameters	Level-1	Level-2	Level-3
Standby power, DAC	7 (122.5 nm)[a]	10 (175.0 nm)	13 (227.5 nm)
Contact power, DAC	3 (52.5 nm)	5 (87.5 nm)	7 (122.5 nm)
Contact force, mN	100	100	100
Contact time, s	0.002	0.002	0.002
Bonding power, DAC	27 (472.5 nm)	35 (612.5 nm)	43 (752.5 nm)
Bonding force, mN	80	80	80
Bonding time, s	0.006	0.006	0.006
Substrate temperature, °C	175	175	175

[a]Ultrasonic amplitudes of capillary tip are listed in brackets.

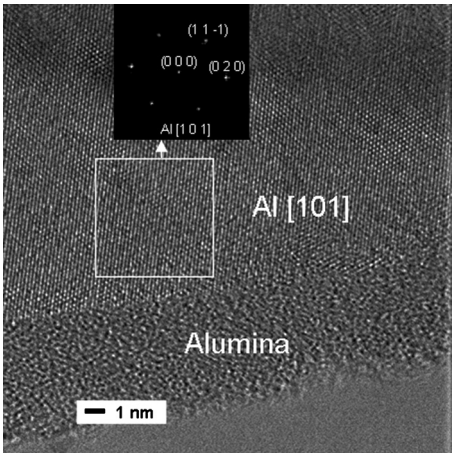

FIG. 1. A uniform amorphous native alumina overlayer (approximately 5 nm thick) envelops an Al pad.

fects on interfacial characteristics, the bonded samples were removed immediately from the work stage, but inevitably maintained a temperature near 175 °C for ~5 s.

Cross-sections of the Au–Al bonds were prepared by dual-beam focused ion beam thinning for scanning electron microscopy (STEM) and TEM. The native alumina film on the metal pad was studied with HRTEM before bonding. The nanostructure at the interface including alumina and IMCs, were investigated by TEM combined with energy dispersive x-ray spectrometry (EDX). TEM analysis was carried out using a JEOL 2100F system at 200 kV. A microprobe beam (0.7 nm diameter) was used for composition analysis with EDX in STEM mode. Fast Fourier transforms (FFTs) of lattice images calculated using IMAGEJ 1.42Q (Ref. 32) and selected area electron diffraction (SAD) were employed to identify Au–Al IMCs.

Shear tests were conducted with a DAGE 4000 microtester at a tool height of 3 μm to evaluate the bonding strength as a function of applied ultrasonic power. The shear strength was expressed as shear force per unit area.

III. RESULTS

A. Characterization of alumina film on Al pads prior to bonding

The typical uniform amorphous alumina film adhering to crystalline Al pads prior to bonding is approximately 5 nm thick (Fig. 1). Because the oxide overlayer is compact and uniform, further oxidation of the pad is passivated, but will be detrimental to bonding as it is a barrier to metal diffusion.

B. Interfacial characteristics of Au–Al bonds

In cross-section, the Au–Al interface consists of two regions, labeled A (without Au–Al IMCs) and B (with IMCs) [Fig. 2(a)]. Region A presents as an approximately 4 nm thick uniform layer between the metals [Fig. 2(b)], whose main constituents are aluminum and oxygen (Table III), consistent with the preservation of the amorphous alumina film, that limits interdiffusion and retards the formation of IMCs. Since the alumina/gold boundaries remain distinct at the atomic scale, limited interfacial diffusion is occurring. This

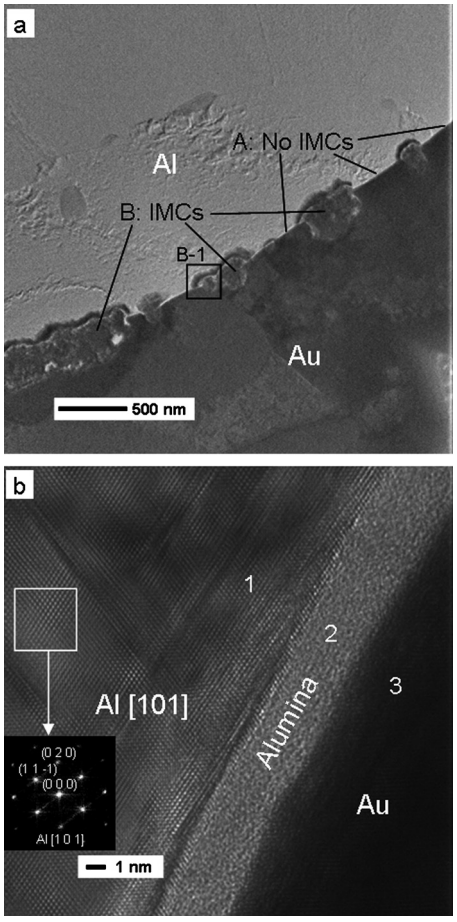

FIG. 2. (a) Overview bright field TEM image of the Au–Al interface in the as-bonded state (see level-2 in Table II for detailed bonding parameters). (b) Details of an A region shows a uniform layer of amorphous alumina remained after ultrasonic bonding, demonstrating lower power thermosonic treatment could not completely disrupt the oxide overlayer.

is consistent with the mechanism of Chang *et al.*[33] who derived a model based on Mott's electron tunneling and ion migration, rather than the diffusion of neutral metal atoms that obey Fick's law. The connectivity of alumina to gold will contribute to bond strength as discussed later, as will other defects induced during thermosonic bonding [Figs. 1 and 2(b)].

TABLE III. STEM-EDX results for regions 1–3 in Fig. 2(b) and 4–10 in Fig. 3(a). The precision of EDX measurement of O is approximately ±10%, and Al, Au approximately ±2%.

Regions	O *K* (at. %)	Al *K* (at. %)	Au *L* (at. %)
1	5	94	1
2	53	45	2
3	2	9	89
4	6	90	4
5	10	59	31
6	45	39	16
7	38	46	16
8	17	22	61
9	11	24	65
10	5	8	87

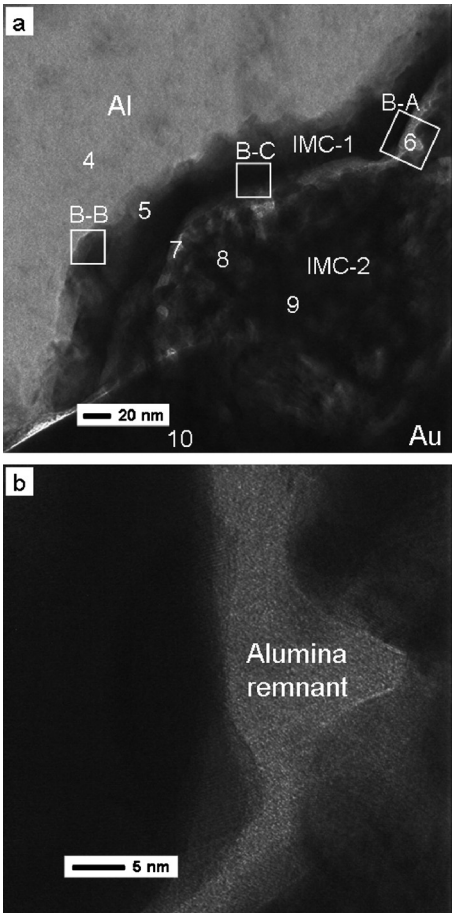

FIG. 3. (a) Details of region B-1 in Fig. 2(a) presenting IMCs formed after ultrasonic bonding. (b) Higher magnification of region B-A showing an alumina remnant encapsulated by IMC-1 ($AuAl_2$) and IMC-2 (Au_4Al).

In region B, chemical reactions dilate the interface to a trilayer 150–300 nm thick [Fig. 3(a), Table III]. Near the pad is an aluminum-rich alloy IMC-1, while there is a gold-rich alloy IMC-2 abutting the Au wire with a distinct microstructure and morphology. In addition, there is a mid-region of relatively light contrast, confirmed as amorphous alumina [Fig. 3(b)]. These alumina remnants inside IMCs are fragmented and distinct from the uniform amorphous layer in the regions without IMCs [Fig. 2(b)], consistent with film disintegration during bonding that accompanied and facilitated the formation of IMC-1 and IMC-2. Karpel *et al.*[34] reported a similar low contrast region with TEM, but without the benefit of chemical analysis, they characterized this feature as a void line. In the materials studied here, the Au–Al bond contains few cavities, and these only exist in the center of large relic alumina ($\geq$20 nm) (Fig. 4), but generally such debris were 5–10 nm in diameter and pore-free.

C. Identification of IMCs formed at the interface

In IMC-1 [Fig. 3(a)] two locations with ordered atomic arrays were selected (B-B and B-C) and lattice images collected [Figs. 5(a) and 5(b)]. FFT analysis was consistent with $AuAl_2$ [001] ($Fm\bar{3}m$, a=5.9988 Å) (Ref. 22) joined with Al ($Fm\bar{3}m$, a=4.0496 Å) (Ref. 35) in B-B, while in B-C, $AuAl_2$ [101] is linked to alumina; the change in IMC texture may be

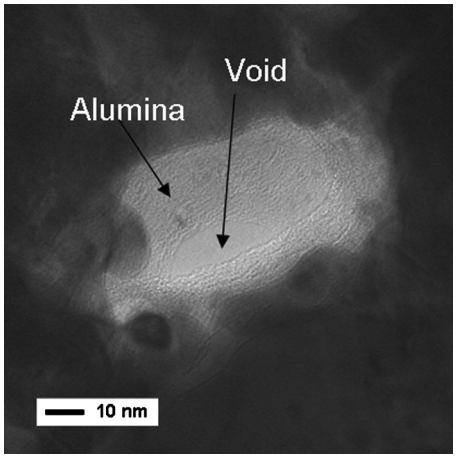

FIG. 4. Voids sometimes form within large relic alumina particles, due to shrinkage of the oxide that accompany partial redaction and inclusion of Al in the IMCs or loss of oxygen.

related to preferential growth during bonding. As further confirmation, SAD of IMC-1 was found to be polycrystalline $AuAl_2$ (although inevitably coexisting with Al reflections as the patterns were collected from a diameter of ~100 nm) [Fig. 6(a)]. In IMC-2 the ring patterns could be indexed as Au_4Al [Fig. 6(b)]. These combined crystallochemical analyses demonstrate that IMC-1 is an aluminum-rich alloy ($AuAl_2$) and IMC-2 a gold-rich alloy (Au_4Al).

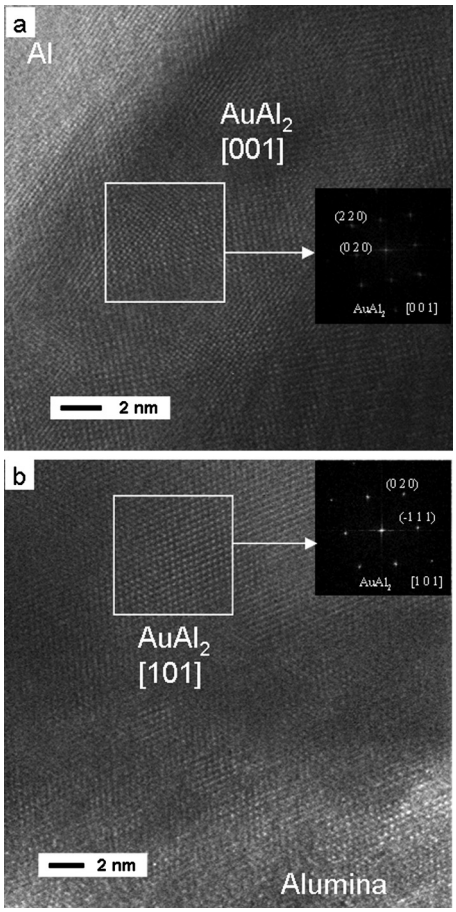

FIG. 5. HRTEM images and Fourier reconstructed patterns of (a) region B-B in Fig. 3(a) with $AuAl_2$ [001] and (b) region B-C in Fig. 3(a) with $AuAl_2$ [101].

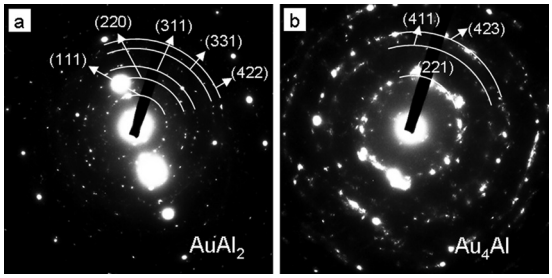

FIG. 6. SAD patterns of (a) IMC-1—$AuAl_2$ and (b) IMC-2—Au_4Al. In pattern (a) strong systematic diffraction rows arise from the aluminum pad.

D. Effect of ultrasonic power

The interfaces of Au/Al formed using three ultrasonic settings are presented in Fig. 7, with the quantity of IMCs at the interfaces increasing significantly at higher ultrasonic power levels. In particular, level 3 (43 DAC) resulted in an almost continuous layer of IMCs, as compared to levels 1 (27 DAC) and 2 (35 DAC), where slightly enhanced connected areas may be due to softening. There is obvious shear strength enhancement with increasing ultrasonic power (Fig. 8).

IV. DISCUSSION

A. Effect of alumina film on thermosonic Au wire bonding

In an analogous manner to copper wire bonding on Al pads,[36] Au–Al bonds also consist of two types of interfacial connection: (i) a continuous and compact alumina film—a native oxide initially present on Al pads—in contact directly with Au [region A, Fig. 2(a)] and (ii) regions containing IMCs (150–300 nm thick) with residual alumina at their core [region B, Fig. 2(a)]. The alumina film in the former case remains intact, indicating that thermosonic bonding did not perturb those regions significantly, without fracturing and relocation of the overlayer. It is possible that alumina/gold interfaces are detrimental toward bonding strength, as IMCs are absent because Au and Al cannot penetrate the alumina barrier [Fig. 2(b)]. However, intense ultrasonic treatment displaces and fragments the alumina film which opens diffusion paths for the metals to migrate and react. In this manner, ultrasonic treatment initiates localized IMC formation and significantly enhances overall bond strength.

B. Effect of ultrasonic power

The application of ultrasonics improves interfacial bonding and adhesion, by initiating alumina disintegration, thereby increasing Al and Au mobility and the rate of IMC formation. This is attributed to the local disintegration of alumina, that determines the rate of formation of IMCs. The ease of IMC interfacial crystallization increases in tandem with ultrasonic power (Fig. 7), and as does bonding strength (Fig. 8). Areas of direct contact of alumina with Au will contribute to bonding but is less significant than the role played by IMCs.

C. Kinetics of Au–Al bond formation

The thermodynamics and kinetics of Au–Al bond formation are difficult to evaluate *in situ* and poorly understood. If IMC growth during annealing is diffusion-limited it follows a parabolic law[28,29,37] such that,

$$x = (Dt)^{1/2} \tag{1}$$

and

$$D = D_0 \exp(-Q/RT), \tag{2}$$

where x is the IMC thickness at time t, D the growth rate constant, D_0 a prefactor, Q the activation energy, R the molar gas constant, and T the absolute temperature.

According to Philofsky,[37] $Q=66.5$ KJ/mol and $D_0 = 5.2\times10^{-8}$ m^2/s for the growth of Au–Al IMCs in butt-welded (635 μm gold wire to 635 μm aluminum wire) diffusion couples during annealing at 200–460 °C. By introducing these parameters to the present work, where $T=175$ °C and $t=5$ s, the IMC thickness x can be estimated as 60–70 nm. However, the observed layer was much thicker

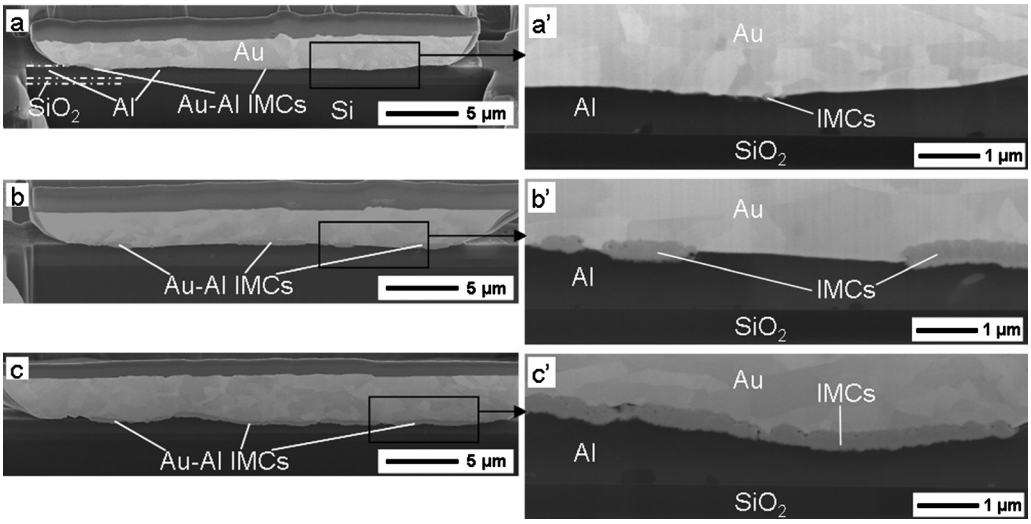

FIG. 7. Dependence of IMC formation on ultrasonic power: (a,a′) level 1<(b,b′) level 2<(c,c′) level 3 (see Table II for detailed parameters). The IMC interlayer becomes contiguous with increasing ultrasonic disruption of the alumina barrier layer.

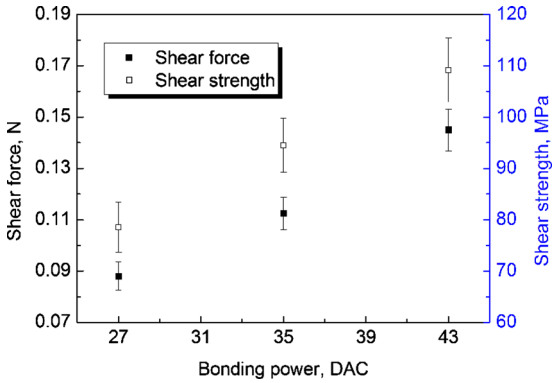

FIG. 8. (Color online) Higher ultrasonic power promotes IMCs of greater structured integrity that increases shear force and shear strength. The error bars are the standard deviation for 20 measured samples.

(150–300 nm), suggesting the main IMC body was formed prior to annealing. If the bonding process is diffusion controlled and occurs in 0.008 s (Table II), this implies D will be $\sim 5.0\times10^{-12}$ m^2/s. Although there is no diffusivity data for gold in liquid aluminum, the diffusion rates of Cu, Ni, Fe, Co, and Ga in this medium at 661 °C are 5.1×10^{-9} m^2/s, 3.3×10^{-9} m^2/s, 2.5×10^{-9} m^2/s, 2.4×10^{-9} m^2/s, and 6.5×10^{-9} m^2/s, respectively.[38] Moreover, it is known that Au (atomic radius=0.1442 nm) diffusion in Al (0.1432 nm) is much quicker than Cu (0.1278 nm) due to the similarity in atomic size.[39] From this it may be inferred that the diffusion rate of Au in liquid Al (at 661 °C) will be larger than 5.1×10^{-9} m^2/s, but during wire bonding, which is a solid state process, it is likely to be three (or four) orders of magnitude as smaller (5.0×10^{-12} m^2/s).

If the values of Q and D_0 from Philofsky[37] are valid for bonding, the effective (or equivalent) temperature obtained from Eq. (2) is 619 °C and includes a thermal contribution arising from mechanical vibration plus a decrease in Q from ultrasonic action. An *in situ* measurement of interfacial temperature using K-type thin film thermocouples yielded 320 °C,[40] the highest found for wire bonding. This is in contrast to the present estimate for small local regions after IMCs reached a significant thickness, while the thermocouple result averages over a large area (20 μm wide, 1 μm thick). In any case, the actual interface temperature must not exceed the melting point of aluminum (660 °C) and the lowest eutectic (525 °C at Au 78 at. %). Consequently, the high effective temperature derived from Eqs. (1) and (2) must be accounted for by a reduction in Q.

Ultrasonics may lower Q if microslip between the Au ball and substrate creates vacancies by increasing the average thermal displacements and diffusivity of atoms. This can also produce large numbers of grain boundaries and dislocations in the IMCs, gold ball and aluminum pad, that provide pathways for rapid metal migration, as grain boundary diffusion invariably has a smaller activation energy than for the bulk diffusion. Below the Tamman temperature (about one-half to two-thirds the melting point in kelvin), atomic diffusion is not principally a bulk process, but is controlled by grain boundaries and other defects.[41] For growth of IMCs ($AuAl_2$ and Au_4Al), this critical temperature is estimated (using the $AuAl_2$ melting point of 1060 °C) to be 394–615 °C, close to or higher than the real interfacial temperature, so grain boundary diffusion may be the rate limiting mechanism. Initially, amorphous alumina oxide is fragmented by ultrasonic vibration, exposing fresh Al surfaces that directly contact Au, and promote crystallization of IMCs; further growth requires metal migration through the IMCs. Xu *et al.*[28] found that Au is the predominant diffusant in the Au–Al system by tracking movements of oxygen in the interface using secondary ion mass spectrometry depth profiling. Therefore, Au diffusion through IMCs ultimately governs their growth which will be accelerated if more boundaries are available. IMC crystals formed during ultrasonic bonding are small (a few tens of nanometers), resulting in large grain boundary surfaces for atomic diffusion. In addition, there may be synergistic effects that dynamically create interfacial vacancies to accelerate diffusion.

IMC formation may also be mediated by dislocation diffusion. Li *et al.*[42,43] demonstrated that ultrasonic vibration during wire bonding generated dislocations in aluminum pads that may promote migration. However, in this study, local IMC formation did not always accompany the creation of a dislocation network in aluminum, as alloys could be absent from nearby areas [Fig. 2(b)]. An alternative explanation is that the initial formation of IMCs depends on oxide rupture by vibration at certain pressures and temperatures, and alloy growth is sustained by Au and Al migration along grain boundaries and dislocations within the alloys themselves.

The sequence of IMC crystallization may be related to their respective effective heats of formation, that reflect the free energy change for the system, as the entropy during solid state interaction will be almost constant.[44] Pretorius *et al.*[27,45] propose that the first-formed phase will process the most negative effective heat of formation at the composition with the lowest eutectic temperature (or liquidus). This is termed the effective composition and in the Au–Al joint corresponds to 78 at. % Au and 22 at. % Al. The calculated effective heats of formation ΔH obtained by Pretorius *et al.*[27] for Au_5Al_2, Au_2Al, Au_4Al, AuAl, and $AuAl_2$ are listed in Table I. As the difference between Au_5Al_2 (−20.0 kJ/mol) and Au_2Al (−19.8 kJ/mol) is negligibly small thermodynamically, either could be the preferable and primary intermetallic. In thin film studies (where Al and Au films were deposited one by one without breaking the vacuum) x-ray diffraction and Rutherford backscattering spectrometry found Au_5Al_2 was the formed initially,[28–30,46] while elsewhere Au_5Al_2 and Au_2Al reportedly grew simultaneously.[47] During annealing, Majni *et al.*[30] found that Au_2Al was the second phase to appear while Xu *et al.*[28,29] showed that Au_4Al was formed after Au_5Al_2. Although there is uncertainty regarding the order of the IMC crystallization, Au_5Al_2, Au_2Al, and Au_4Al are undoubtedly the dominant phases formed in thin solid film systems. It is reported that $AuAl_2$ is not favored, and observed only after prolonged annealing of thin Au on bulk Al,[30] however, the present study found that Au_4Al and $AuAl_2$ simultaneously encase the alumina remnants (Fig. 4).

Interfacial reaction during wire bonding is inherently nonequilibrium, aggravated through the application of ultra-

sonic vibration, with chemical gradients influenced by oxides, defects, and atomic mobility. The coexistence of $AuAl_2$ and Au_4Al is a consequence of relic alumina separating IMC interfaces, which limit Au diffusion and to a lesser extent Al mobility. Thus, the effective concentration of Au at the growth interface adjacent to Al is lower than in an ideal thin film system.[28–30] By supposing the effective concentration of Au at the Al interface is 33 at. %, the effective heat of formation for $AuAl_2$, AuAl, Au_2Al, Au_5Al_2, and Au_4Al can be recalculated using the model of Pretorius[27,45] (Table I). Thus, $AuAl_2$ ($\Delta H' = -30.7$ kJ/mol) is favored between aluminum and alumina remnant. Similarly, the higher effective concentration of Au at the growth interface adjacent to Au results in Au_4Al ($\Delta H'' = -19.0$ kJ/mol) readily forming (Table I). Although ΔH is a reasonable indirect measure of Gibbs'-free energy release during interfacial reactions, the role of nucleation barriers and kinetics[27,45,48–50] are of most consequence in predicating the phase assemblage in the bond. Pretorius *et al.*[27] stated that the more atoms in a unit cell, the more difficult and less energetically favorable it is to crystallize. Au_8Al_3 has 44 atoms per unit cell and longer range order, and will not readily form, especially in the nonequilibrium situation of ultrasonic wire bonding, where growth occurs at a moving interface. (As noted earlier Au_5Al_2 is probably equivalent to Au_8Al_3.) Taking nucleation into consideration, it is reasonable to believe $AuAl_2$ and Au_4Al are formed first during wire bonding, while earlier reports of Au_8Al_3/Au_5Al_2 remain speculative, as the characterization of the latter were not substantiated by diffraction analysis. Furthermore, differentiating Au_8Al_3 from Au_5Al_2 by microanalysis would be challenging as the crystals produced during bonding are smaller than the analytical volume.

D. Thermosonic bonding mechanism

To summarize, the mechanism of thermosonic gold wire bonding is illustrated in Fig. 9. Ideally, both the aluminum pad and gold wire are perfectly clean and when joined thermally there is greater diffusion of Au into Al; this yields a gold-rich alloy that is notionally Au_5Al_2 ($R\bar{3}c$) but more likely a disordered cubic ($Fm\bar{3}m$) solid solution. Ultrasonic power creates dislocations and grain boundaries in the pad and wire as well as the IMCs that accelerate metal migration leading to thicker IMC layers and stronger bonds. In real systems the surface of the pad is invariably oxidized and the amorphous alumina is a barrier to Au and Al interdiffusion leading to inferior interconnects. $AuAl_2$ ($Fm\bar{3}m$ and 12 atoms per unit cell) and Au_4Al ($P2_13$ and 20 atoms per unit cell) are formed due to the limiting of Au and Al diffusion by alumina. Ultrasonic vibration fragments the alumina and provides many grain boundary pathways along which the metals diffuse and react. At the IMC boundary, it is likely that the Au and Al are disordered and correspond to $Pm\bar{3}m$ simple cubic periodicity with 2 atoms per unit cell. In general, both the initial alumina and the debris are compact, but in larger relic alumina regions voids are sometimes observed.

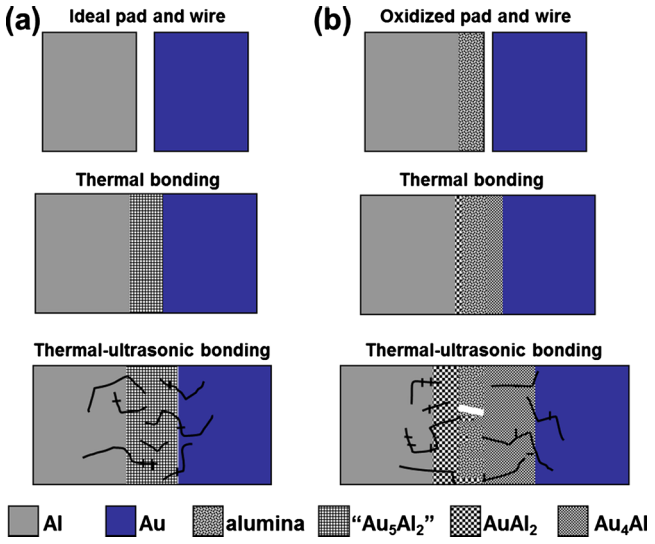

FIG. 9. (Color online) The crystal chemistry and strength of interconnects depends on the nature of pad and wire surfaces and whether ultrasonic vibration is applied together with heating. (a) In the ideal situation both the aluminum pad and gold wire are perfectly clean. When joined thermally there is greater diffusion of Au into Al than vice versa and an IMC notionally identified as Au_5Al_2 formed. With the application of ultrasonic power dislocations in the pad, wire and IMCs accelerate metal mobility leading to thicker IMC layers and a stronger bond. (b) In real systems, the pad surface is invariably oxidized and the amorphous alumina will act as a barrier to Au and Al interdiffusion leading to inferior interconnects. Ultrasonic vibration fragments the alumina and provides many grain boundary pathways through which the metals diffuse and react. $AuAl_2$ ($Fm\bar{3}m$ and 12 atoms per unit cell) and Au_4Al ($P2_13$ and 20 atoms per unit cell) rather than Au_5Al_2 are formed due to the limiting Au and Al diffusion by alumina.

V. CONCLUSIONS

The crystallochemical and physical interfacial characteristics of interconnects (alumina, IMCs and defects) during thermosonic bonding of gold wires on aluminum pads were correlated with ultrasonic energy, interfacial structure and bonding strength. It is shown that:

(1) A compact amorphous alumina layer ~5 nm thick is present on aluminum prior to bonding and acts as a barrier to Au and Al interdiffusion.
(2) Ultrasonic vibration partially disrupts the continuity of the alumina film to create favorable diffusion pathways that promote the local formation of IMCs. At higher ultrasonic energies, alumina fragmentation is greater, metal mobility accelerates, and IMCs more readily form in the contact area, resulting in a stronger bond. The dominant alloys are Au_4Al and $AuAl_2$ (total thickness of 150–300 nm), with remnant alumina encapsulated in these IMCs.
(3) With the simplifying assumption that IMC formation during bonding is diffusion controlled, we estimate the ultrasonic effect in the current work to be equivalent to heating the interface to >600 °C, while the overall average temperature is probably near 320 °C. This arises because ultrasonic vibration increases the real local temperature and simultaneously produces numerous diffusion pathways via grain boundaries and dislocations that lower activation energies.

(4) The coexistence of Au_4Al and $AuAl_2$ is due to a native alumina overlayer that attenuates Au and Al interdiffusion. This reduces the effective concentration of Au at the growth interface adjacent to Al and that of Al at the interface near Au.

ACKNOWLEDGMENTS

This research was funded as a PMI2 Project (Grant No. RC 41) through the UK Department for Innovation, Universities and Skills (DIUS).

[1]A. P. Hulst, and C. Lasance, Weld. J. (Miami, FL, U.S.) **57**, 19 (1978).
[2]R. D. Mindlin, ASME Trans. J. Appl. Mech. **18**, 331 (1951).
[3]G. G. Harman and J. Albers, IEEE Trans. Parts Hybrids Packag. **13**, 406 (1977).
[4]B. Langenecker, IEEE Trans. Sonics Ultrason. **13**, 1 (1966).
[5]G. G. Harman, *Wire Bonding in Microelectronics:Materials, Processes, Reliability, and Yield*, 2nd ed. (McGraw-Hill, New York, 1997).
[6]J. Qi, N. C. Hung, M. Li, and D. Liu, Scr. Mater. **54**, 293 (2006).
[7]H. Huang, A. Pequegnat, B. H. Chang, M. Mayer, D. Du, and Y. Zhou, J. Appl. Phys. **106**, 113514 (2009).
[8]I. Lum, H. Huang, B. H. Chang, M. Mayer, D. Du, and Y. Zhou, J. Appl. Phys. **105**, 024905 (2009).
[9]J. L. Murray, H. Okamoto, and T. B. Massalski, Bull. Alloy Phase Diagrams **8**, 20 (1987).
[10]R. F. Hoyt and A. C. Mota, J. Less-Common Met. **62**, 183 (1978).
[11]M. Ellner, U. Kattner, and B. Predel, J. Less-Common Met. **170**, 171 (1991).
[12]E. A. Owen and E. A. O'Donnell Roberts, J. Inst. Met. **71**, 213 (1945).
[13]O. E. Ullner, Ark. Kemi, Mineral. Geol. **A14**, 1 (1940).
[14]H. Büchler and K.-J. Range, J. Less-Common Met. **161**, 347 (1990).
[15]V. G. Kuznecov and V. I. Rabezova, Dokl. Akad. Nauk SSSR **81**, 51 (1951).
[16]L. Tertian and D. Darmagna, Mem. Sci. Rev. Metall. **62**, 207 (1965).
[17]M. Ellner, Z. Kristallogr. **162**, 69 (1993).
[18]K. J. Range and H. Buechler, J. Less-Common Met. **154**, 251 (1989).
[19]M. Puselj and K. Schurt, J. Less-Common Met. **35**, 259 (1974).
[20]G. K. Abramyan, A. N. Pilyankevich, and I. N. Frantsevich, Dokl. Akad. Nauk SSSR **196**, 1054 (1971).
[21]K. Frank and K. Schubert, J. Less-Common Met. **22**, 349 (1970).
[22]H. Buechler and K. J. Range, J. Less-Common Met. **160**, 143 (1990).
[23]W. W. Warren, Jr., R. W. Shaw, Jr., A. Menth, F. J. DiSalvo, A. R. Storm, and J. H. Wernick, Phys. Rev. B **7**, 1247 (1973).
[24]M. Ellner, U. Kattner, and B. Predel, J. Less-Common Met. **87**, 305 (1982).
[25]C. D. West and A. W. Peterson, Z. Kristallogr. **88**, 93 (1993).
[26]F. R. De Boer, R. Boom, W. C. M. Mattens, A. R. Miedema, and A. K. Niessen, *Cohesion in Metals* (North-Holland, Amsterdam, 1988).
[27]R. Pretorius, A. M. Vredenberg, and F. W. Saris, J. Appl. Phys. **70**, 3636 (1991).
[28]C. Xu, T. Sritharan, and S. G. Mhaisalkar, Scr. Mater. **56**, 549 (2007).
[29]C. Xu, T. Sritharan, and S. G. Mhaisalkar, Thin Solid Films **515**, 5454 (2007).
[30]G. Majni, C. Nobili, G. Ottaviani, M. Costato, and E. Galli, J. Appl. Phys. **52**, 4047 (1981).
[31]M. H. Francombe, A. J. Noreika, and W. J. Takei, Thin Solid Films **1**, 353 (1968).
[32]W. Rasband, IMAGEJ Version 1.42q, National Institutes of Health, Bethesda, Maryland, USA, 2009, http://rsb.info.nih.gov/ij
[33]C. C. Chang, T. A. Callcott, and E. T. Arakawa, Phys. Rev. B **32**, 6138 (1985).
[34]A. Karpel, G. Gur, Z. Atzmon, and W. Kaplan, J. Mater. Sci. **42**, 2334 (2007).
[35]R. T. Downs and M. Hall-Wallace, Am. Mineral. **88**, 247 (2003).
[36]H. Xu, C. Liu, V. V. Silberschmidt, S. S. Pramana, T. J. White, and Z. Chen, Scr. Mater. **61**, 165 (2009).
[37]E. Philofsky, Solid-State Electron. **13**, 1391 (1970).
[38]Y. Du, Y. A. Chang, B. Huang, W. Gong, Z. Jin, H. H. Xu, Z. H. Yuan, Y. Liu, Y. H. He, and F. Y. Xie, Mater. Sci. Eng., A **363**, 140 (2003).
[39]S. Murali, N. Srikanth, and C. J. Vath III, Mater. Res. Bull. **38**, 637 (2003).
[40]J. Ho, C. Chen, and C. Wang, Sens. Actuators, A **111**, 188 (2004).
[41]M. A. Nicolet, Thin Solid Films **52**, 415 (1978).
[42]J. Li, L. Han, J. Duan, and J. Zhong, Appl. Phys. Lett. **90**, 242902 (2007).
[43]J. Li, F. Wang, L. Han, and J. Zhong, J. Phys. D: Appl. Phys. **41**, 135303 (2008).
[44]O. Kubaschewski and C. B. Alcock, *Metallurgical Thermochemistry* (Pergamon, Oxford, 1979).
[45]R. Pretorius, C. C. Theron, A. C. Vantomme, and J. C. Mayer, Crit. Rev. Solid State Mater. Sci. **24**, 1 (1999).
[46]J. M. Berg and R. A. Hamm, J. Vac. Sci. Technol. **19**, 156 (1981).
[47]S. U. Campisano, G. Foti, E. Rimini, S. S. Lau, and J. W. Mayer, Philos. Mag. **31**, 903 (1975).
[48]K. N. Tu, Annu. Rev. Mater. Sci. **15**, 147 (1985).
[49]A. M. Gusak and G. V. Lucenko, Acta Mater. **46**, 3343 (1998).
[50]F. Hodaj and A. M. Gusak, Acta Mater. **52**, 4305 (2004).